Biochimica et Biophysica Acta 1848 (2015) 532–543

Contents lists available at ScienceDirect

Biochimica et Biophysica Acta

journal homepage: www.elsevier.com/locate/bbamem

Effect of lamellarity and size on calorimetric phase transitions in single component phosphatidylcholine vesicles

Jelena Drazenovic [a], Hairong Wang [a], Kristina Roth [a], Jiangyue Zhang [b], Selver Ahmed [a], Yanjing Chen [c], Geoffrey Bothun [c], Stephanie L. Wunder [a,*]

[a] Department of Chemistry, Temple University, Philadelphia, PA 19122, USA
[b] Department of Chemistry, Immaculata University, Immaculata, PA 19345, USA
[c] Department of Chemical Engineering, University of Rhode Island, Kingston, RI 02881, USA

ARTICLE INFO

Article history:
Received 23 May 2014
Received in revised form 26 September 2014
Accepted 1 October 2014
Available online 22 October 2014

Keywords:
Vesicle lamellarity
Unilamellar vesicle
Gel-to-liquid phase transition temperature
Vesicle curvature
DMPC
Coupled phase transition

ABSTRACT

Nano-differential scanning calorimetry (nano-DSC) is a powerful tool in the investigation of unilamellar (small unilamellar, SUVs, or large unilamellar, LUVs) vesicles, as well as lipids on supported bilayers, since it measures the main gel-to-liquid phase transition temperature (T_m), enthalpies and entropies. In order to assign these transitions in single component systems, where T_m often occurred as a doublet, nano-DSC, dynamic light scattering and cryo-transmission electron microscopy (cryo-TEM) data were compared. The two T_ms were not attributable to decoupled phase transitions between the two leaflets of the bilayer, i.e. nano-DSC measurements were not able to distinguish between the outer and inner leaflets of the vesicle bilayers. Instead, the two T_ms were attributed to mixtures of oligolamellar and unilamellar vesicles, as confirmed by cryo-TEM images. T_m for the oligolamellar vesicles was assigned to the peak closest to that of the parent multilamellar vesicle (MLV) peak. The other transition was higher than that of the parent MLVs for 1,2-dimyristoyl-*sn*-glycero-3-phosphocholine (DMPC), and increased in temperature as the vesicle size decreased, while it was lower in temperature than that of the parent MLVs for 1,2-dipalmitoyl-*sn*-glycero-3-phosphocholine (DPPC), and decreased as the vesicle size decreased. These subtle shifts arose due to small differences in the values of ΔH and ΔS, since T_m is determined by their ratio ($\Delta H/\Delta S$). It was not possible to completely eliminate oligolamellar structures for MLVs extruded with the 200 nm pore size filter, even after 120 passes, while these structures were eliminated for MLVs extruded through the 50 nm pore size filter.

© 2014 Elsevier B.V. All rights reserved.

1. Introduction

Liposomes are frequently used as surrogates for cellular membranes in basic studies, as nanoscale reactors, as sensors, and in biotechnology applications. Supported lipid bilayers (SLBs) on both planar and nanoparticle substrates have been investigated for similar reasons. Among the many techniques that have been used for characterization of lipid morphology, differential scanning calorimetry (DSC) [1] and nano-DSC provide sensitive means of detecting phase transition temperatures, such as the gel (L_β) to liquid-crystal (L_α), T_m, of lipid vesicles, and their associated enthalpies and entropies, which reflect their packing properties (interactions) and alkyl chain conformations.

Liposomes are self-closing spherical particles consisting of lipid bilayers that encapsulate the solvent. They can be prepared [2] as multilamellar vesicles (MLVs) [3], which consist of concentric bilayer spheres, or can be formed into giant (GUVs, >1 μm diameter) [4], large (LUVs, >100–200 nm to 1 μm in diameter) [2], small (SUVs, 20 to 50 nm diameter) unilamellar and bilamellar vesicles [5]. Smaller vesicles are prepared by sonication [6,7], centrifugation/ultracentrifugation [8,9], gel filtration [10], and extrusion of MLVs [11–16] or GUVs [17]. A combination of freeze/thawing (to break up large MLVs [18]) followed by extrusion techniques [19] is often used. Formation of unilamellar vesicles occurs by a process of membrane rupture and resealing during which there can be entrapment of small vesicles (multivesicular (MVVs) or oligovesicular vesicles) and some lamellarity can be maintained (oligolamellar vesicles). The freeze–thaw (above T_m) procedure before extrusion [19] increases the proportion of unilamellar vesicles by causing internal lamellae of the MLVs to separate and vesiculate, reducing the number of closely associated bilayers passing through the filter, thus reducing the formation of oligolamellar vesicles [13].

Abbreviations: MLVs, multilamellar vesicles; LUVs, large unilamellar vesicles, 100–200 nm; SUVs, small unilamellar vesicles, 15–30 nm; DMPC, 1,2-dimyristoyl-*sn*-glycero-3-phosphocholine; DPPC, 1,2-dipalmitoyl-*sn*-glycero-3-phosphocholine; PC, phosphatidylcholine; PBS, phosphate buffer saline; SLB, supported lipid bilayer; Nano-DSC, nano-differential scanning calorimetry

* Corresponding author.
E-mail address: slwunder@temple.edu (S.L. Wunder).

http://dx.doi.org/10.1016/j.bbamem.2014.10.003
0005-2736/© 2014 Elsevier B.V. All rights reserved.

The latter are evidenced by the fraction of phospholipid exposed to the external medium (using ^{13}P-NMR and chemical shift reagents) [20,21] and cryo-TEM images [13,21,22]. Multivesicular vesicles (MVVs), in which smaller vesicles are contained within larger vesicles have also been prepared as nested nanoreactors [23] or have been observed by cryogenic-transmission electron microscopy (cryo-TEM) when preparing SUVs/LUVs [13,24]. A schematic of unilamellar, oligolamellar and multivesicular vesicles is presented in Fig. 1. Despite the many methods of preparing unilamellar vesicles, and the desirability of forming uniform, well characterized dispersions, a simple method to assess whether unilamellarity is achieved is not available.

For single component lipid systems, multilamellar vesicles typically show a narrow, main gel-to-liquid crystal phase transition (T_m) and a lower temperature pretransition (T_{pre}) characteristic of the ripple phase. Large unilamellar vesicles (LUVs) and small unilamellar vesicles (SUVs) show a typically broadened main phase transition, which can appear at slightly higher or lower temperatures [25,26], a broadened pretransition [27,28], and enthalpies of melting lower than those of the parent MLVs [29]. Similar changes have been observed for lipids on nanoparticle supports, where T_m broadens and shifts to a temperature lower than for the parent MLVs, and there is no pretransition [30]. Double transitions, assigned to the proximal (near surface) and distal leaflets of single component planar bilayers, have also been observed [31].

In order to use nano-differential scanning calorimetry of vesicles to investigate lamellarity, lipid exchange, flip-flop between the inner and outer leaflets, fusion/aggregation phenomena, supported lipid bilayer formation and organization of lipids on solid supports, identification of the calorimetric transitions is critical. However, earlier calorimetry studies were hampered by the instability of the SUV preparations, which fused to form larger bilayer structures, before or during the calorimetry scan [25,32,33].

We have observed multiple peaks in both unilamellar vesicles and SLBs that contain only a single lipid species. There are two possibilities, at least in the case of the single component vesicles. The first is that there are differences in packing between the inner and outer leaflets of the bilayer. The second is that double or multiple bilayers remain, perturbing the interactions between the single bilayers. As shown in Fig. 1, the lipid headgroups can be in contact with bulk water, or can interact with interstitial water and be constrained on one or both sides by another lipid bilayer. In order to determine the reason for the observation of more than one peak in the calorimetry traces of single component vesicles, SUVs/LUVs were prepared using well known procedures, namely by sonication, freeze–thawing and extrusion. The morphology of the LUVs viewed by cryo-transmission electron microscopy (cryo-TEM) was compared with nano-DSC runs to determine the origin of the double transitions.

2. Materials and methods

2.1. Materials

1,2-Dimyristoyl-*sn*-glycero-3-phosphocholine (DMPC, 14:0 PC) and DPPC: 1,2-dipalmitoyl-*sn*-glycero-3-phosphocholine (DPPC, 16:0 PC) were obtained from Avanti Polar Lipids (Alabaster, AL) and used without further purification. All solutions/suspensions were prepared with chloroform and HPLC grade water, with or without 0.1 M PBS buffer (100 mM NaCl solution and 2 mM KCl), purchased from Fisher Chemicals (Fairlawn, NJ). An Avanti Mini-Extruder from Avanti Polar Lipids was employed for extrusion of the lipids, using 50, 100, 200 and 400 nm pore size polycarbonate filters.

2.2. Preparation of multilamellar and small/large unilamellar vesicles

The DMPC was dissolved in chloroform and dry lipid films were formed after evaporation of the solutions under a stream of nitrogen and then in a vacuum oven overnight to remove any residual solvent. The lipid film was then redispersed in water or 0.1 M PBS buffer and incubated at a temperature of 45 °C (above T_m of DMPC) or 55 °C (above T_m of DPPC) for 1 h with periodic shaking to form hydrated multilamellar vesicles (MLVs). Large unilamellar vesicles (LUVs) were obtained from the MLVs by successive extrusions (without freeze thawing the MLVs) using first the 400, 200 nm, 100 nm and finally the 50 nm diameter polycarbonate filters. In each case, approximately 1 ml of a 10 mg/ml lipid solution was passed back and forth for a fixed (5×, 20×, 40×, 120×) number of times as described in the text. LUVs/SUVs were also prepared using freeze/thaw cycles and/or sonication. The SUVs were prepared by tip sonication of the MLVs (Fisher Scientific Model 100 Ultrasonic Dismembrator), with 10–15 Watt power in an ice bath to dissipate the heat generated until a clear suspension was obtained, and the titanium dust removed by centrifugation (12,000 for 20 min). The tip sonication was achieved using different pulse sequences, as described below. There was no loss of lipid during the extrusion process, as confirmed by phosphorus analysis [34–36] and LC–MS. After extrusion, additional water or salt solution was added to yield vesicle suspensions of 1 mg/mL.

2.3. Analysis

2.3.1. Dynamic light scattering (DLS)

Dynamic light scattering (DLS) measurements were obtained on a Malvern Zetasizer Nano-ZS (Malvern Instruments Ltd., Malvern, U.K.) at 25 °C. For the temperature dependent measurements, the sample was equilibrated for 1 h before each measurement. Diameters are reported as z-, volume or number averages. The z-average is the intensity weighted effective diameter—the hydrodynamic diameter that a sphere

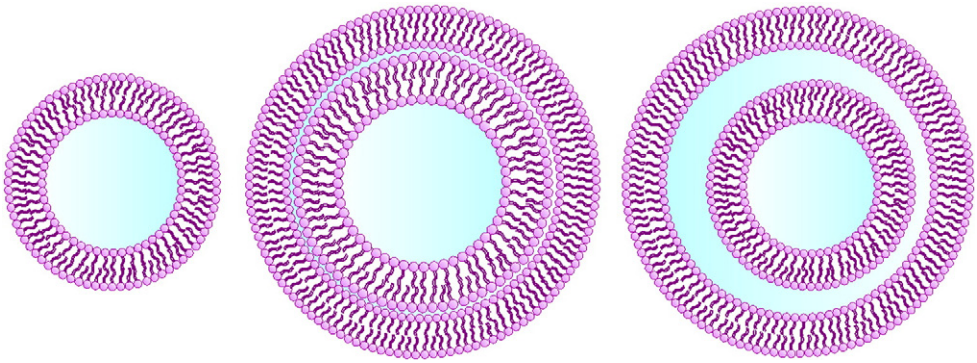

Fig. 1. Schematic of unilamellar, oligolamellar and nested multivesicular (MVV) vesicles.

would have in order to diffuse at the same rate as the particle being measured. The autocorrelation function generated by the DLS measurement is analyzed by cumulant analysis, based on nonlinear least-squares (NLLS) fits of the autocorrelation function with Malvern's Zetasizer *Nano 4.2* software utilizing a version of the CONTIN algorithm [37]. It is a moment expansion that gives as the first two terms the z-average size and a width parameter called the polydispersity index (PDI). The intensity distribution can be converted into a volume distribution or distribution describing the relative proportion of multiple components in a system based on their mass or volume using the Mie scattering theory.

2.3.2. Nano-differential scanning calorimetry (nano-DSC)

Nano-differential scanning calorimetry (nano-DSC) measurements were obtained on a TA Instruments (New Castle, DE) Nano DSC-6300. Samples were scanned at heating/cooling rates of 1 °C/min, using 1–2 mg lipid. Samples were run 5–15 min after preparation, unless otherwise noted, and the first heating and cooling scans are reported. However, the first and second heating scans were identical for the extruded vesicles, and the calorimetry traces remained the same for at least 2 weeks after preparation, when kept at room temperature or above the phase transition temperature of the lipid.

2.3.3. Cryogenic-transmission electron microscopy (cryo-TEM)

The LUVs and supported lipid bilayer suspensions were prepared for cryo-TEM at 25 °C using a Vitrobot (FEI Company), which is a PC-controlled robot for sample vitrification. Quantifoil grids were used with 2 μm carbon holes on 200 square mesh copper grids (Electron Microscopy Sciences, Hatfield, PA). The grid was immersed in the sample, blotted to reduce film thickness, and vitrified in liquid ethane. The sample was then transferred to liquid nitrogen for storage. Imaging was performed using a cooled stage JEOL JEM-2100F TEM (Model 915, Gatan Inc., Pleasanton, CA) at 200 kV. Average sizes by TEM were obtained by analysis of ~50–100 individual unilamellar vesicles.

3. Results

3.1. Nano-DSC data

The nano-DSC data for DMPC MLVs and LUVs prepared by extrusion through a 400 nm polycarbonate filter (40×), or extrusion through a 200 nm (40×) filter and the same sample further extruded through 100 (40×) and 50 nm (40×) polycarbonate filters in water are presented in Fig. 2. The same trends (Supplementary information (SI) Fig. 1 and Table 1) were obtained for vesicles prepared in 0.1 M PBS buffer. A sample (in water) in which the MLVs were freeze–thawed 5×, followed by extrusion with a 100 nm pore size filter 40× had the same nano-DSC trace as the sample extruded using the 200 nm (40×) and 100 nm (40×) pore size filters. Nano-DSC scans for DMPC MLVs tip sonicated for two pulse sequences, 1 min on/30 s off pulse sequence for 15 cycles (~20 min), and 20 s on/10 s off for 55 min total are shown in Fig. 3.

The DMPC MLVs appear as a single asymmetric peak, while the extruded DMPC LUVs are observed at two or one temperature(s), and the sonicated DMPC SUVs also exhibit two peaks. For the extruded/sonicated DMPC LUVs/SUVs: (i) the transition at lower temperature remains approximately constant, at the same temperature as the MLV transition; (ii) the transition at higher temperature shifts to higher temperatures as the pore size of the filter used for extrusion decreases; (iii) the intensity of the high temperature transition increases with respect to that at lower temperature as the pore size of the filter used for extrusion decreases; (iv) the higher temperature peak is the only one observed for LUVs where the 50 nm filter was used; and (v) for the tip sonicated SUVs the transition at higher temperature increases with respect to that at lower temperature (near the MLV transition) as the length of sonication time increases. The width of the peaks,

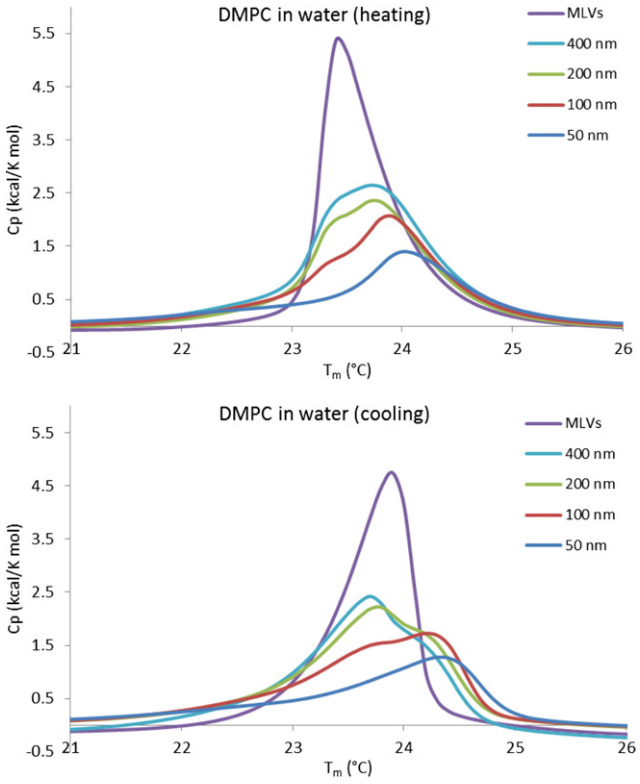

Fig. 2. Nano-DSC plots of DMPC MLVs and LUVs in water extruded sequentially through 200 nm (40×); 100 nm (40×)—same plot was obtained for freeze/thawed MLVs extruded 40× through a 100 nm filter and 50 nm (40×) polycarbonate filters.

particularly the MLV transition, is broader than is observed at slower scan rates. At 0.5 °C/min, $\Delta T_{1/2} = 0.56$ °C [30] and at 0.08 °C/min it is 0.12 °C [38].

When DMPC MLVs are extruded through a 200 nm pore size filter for different numbers of passes, similar trends are observed (Fig. 4); the same results (SI Fig. 2) were obtained with extrusion through the 400 nm filter. The higher temperature peak increases with respect to the lower temperature peak as the number of passes through the extruder increases, but both peaks remain at the same temperatures on both the heating and cooling cycles.

On the heating cycle of the MLVs, the gel-to-liquid phase transition temperature has an abrupt start and a high temperature tail, while on the cooling cycle, the reverse occurs, effects have been attributed to the slow response time of the calorimeter compared with the time scale of the transition [29]. The peak position on the cooling curve is therefore ~0.3–0.5 °C higher than on the heating cycle. However, at slower scan rates (0.5 °C/min), the difference between T_m and T_c is

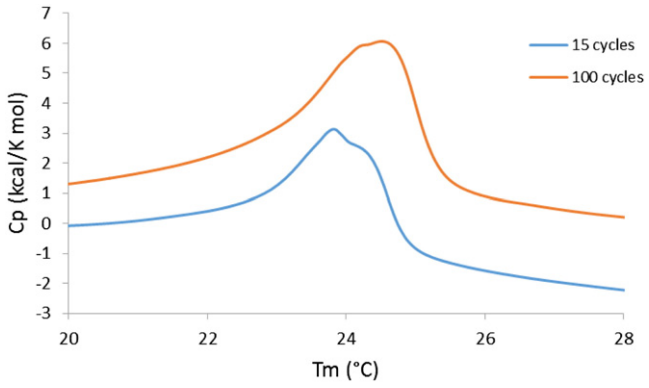

Fig. 3. Nano-DSC plots of tip sonicated DMPC SUVs after 15 and 100 cycles.

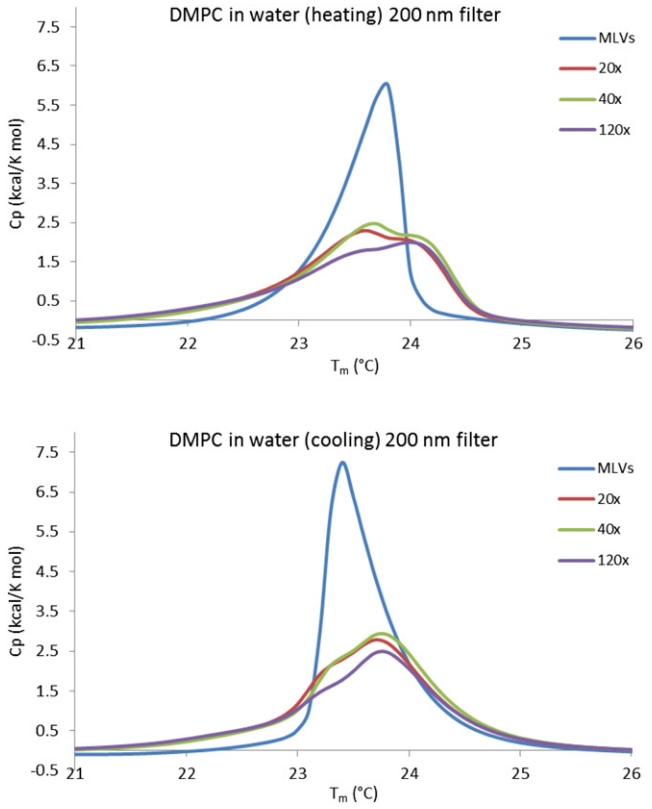

Fig. 4. Nano-DSC plots of DMPC MLVs and LUVs in water extruded 20×, 40× and 120× through 200 nm polycarbonate filters.

only 0.1 °C [30]. In the case of the SUVs/LUVs, the start of the melt transition is more gradual, but the high temperature tail coincides with that of the MLVs. On the cooling cycle, the SUVs/LUVs undergo the liquid crystal-to-gel transition at higher temperatures than the MLVs, and as occurred in that case, the peak transitions on the cooling cycles occur at (~0.3–0.5 °C) higher temperatures than on the heating cycles for both transitions. For SUVs/LUVs extruded with the same pore size filter, the high temperature peak has greater intensity than the low temperature peak on the heating than on the cooling cycle, and as for the MLVs, this is attributed to the slow response time of the calorimeter compared with the time scale of the transition [29].

The T_m, T_c values, and enthalpy change for the gel to liquid crystalline phase transition (for heating, ΔH_m and cooling ΔH_c) for the LUVs and MLVs in water are presented in Table 1. The thermodynamic parameters are for the first heating/cooling cycle, with the run started between 5 and 15 min after preparation. Nevertheless we should stress that the enthalpy values retrieved from the second heating scan increase significantly when samples are held at low temperatures for prolonged periods (although this effect was not investigated in detail). ΔH (total) and ΔS (total) were obtained from the integrated areas of the two nano-DSC peaks for the SUVs/LUVs, obtained on the first heating and cooling cycles. The values of ΔH_m and ΔH_c are the same for the 1st heating/1st cooling cycle of each SUV/LUV or MLV prepared under the same conditions; error bars indicate values obtained for the same sample run 3 times. Further, both ΔH (total) and ΔS (total) decrease with decreased vesicle size, as previously reported for ΔH_m [39]. The values measured here are in reasonable agreement with those for DMPC MLVs (ΔH_m = 5.5–6.2 kcal/mol, including the pretransition [32]) and (sonicated) SUVs (ΔH_m = 3.8 kcal/mol [32, 39]). As in the case of sonicated DODAB vesicles [40], cooling (here for 1 week) at 4 °C resulted in an increase in ΔH, but the shape of the nano-DSC plots remained the same.

When DMPC MLVs are extruded through a 200 nm pore size filter for different numbers of passes, similar trends are observed (Fig. 4); the same results (SI Fig. 2) were obtained with extrusion through the 400 nm filter. The higher temperature peak increases with respect to the lower temperature peak as the number of passes through the extruder increases, but both peaks remain at the same temperatures on both the heating and cooling cycles.

Nano-DSC traces for DPPC (Fig. 5) also show double (but less well defined) transitions for the SUVs/LUVs, but in this case, the phase transition temperature of the higher temperature peak corresponds to that of the parent MLVs, and the phase transition temperature of the lower temperature peak decreases with decreasing pore size of the filters used for extrusion. On the cooling cycle, the transitions cannot be distinguished at this scan rate. Previous nano-DSC data for DPPC obtained at slower scan rates (1 °C/h and 5 °C/h) exhibited better separated transitions with a peak near that of the parent MLV and a broader peak at lower T [28]. The values of ΔH and ΔS (Table 2) both increase with increasing vesicle size. Data for DPPC in water are presented in SI Fig. 3 and Table 2.

Table 1
T_m, T_c and ΔH_m, ΔH_c for DMPC LUVs and MLVs in water.

Pore filter size	50 nm	100 nm	200 nm	MLVs
Heating cycle (1st)				
T_m (peak 1) °C	(22.3)	23.4 ± 0.1	23.4	23.4
T_m (peak 2) °C	24.0	23.9	23.7	
ΔH_m (total) kcal/mol	3.8	4.5 ± 0.3	5.0	5.3
ΔS_m (total) kcal/(mol K)	0.013	0.015	0.017	0.018
ΔS_m (total) J/(mol K)	53.5	63.4	69.9	75.5
Cooling cycle (1st)				
T_c (peak 1) °C	(22.4)	23.8 ± 0.1	23.8	23.9
T_c (peak 2) °C	24.3	24.2	24.2	
ΔH_c (total) kcal/mol	3.5	4.0 ± 0.3	4.8	5.9
ΔS_c (total) kcal/(mol K)	0.011	0.013	0.016	0.02
ΔS_c (total) J/(mol K)	49.5	55.8	67.4	82.6

Error bars indicate repeat of same sample 3 times.

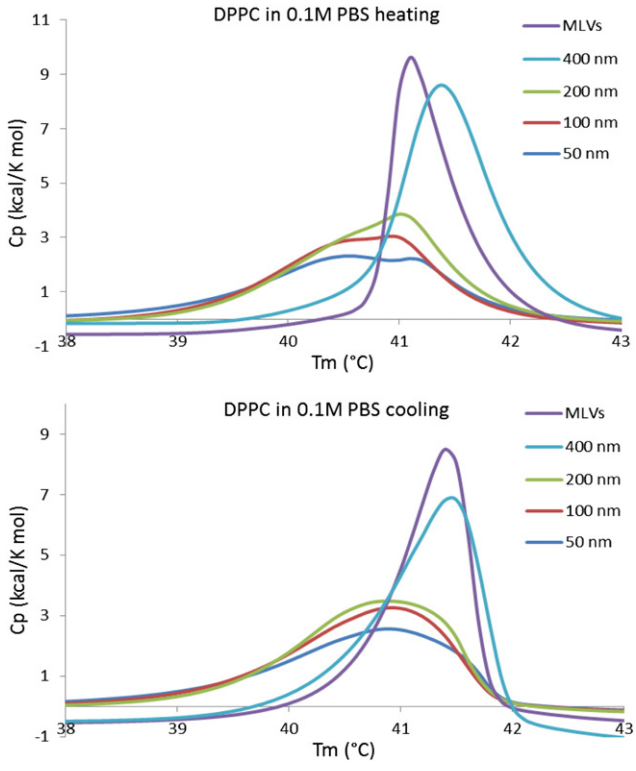

Fig. 5. Nano-DSC plots of DPPC MLVs and LUVs in 0.1 M PBS buffer extruded sequentially 40× each through 400, 200, 100 and 50 nm polycarbonate filters.

Table 2
T_m, T_c and ΔH_m, ΔH_c for DPPC LUVs and MLVs in 0.1 M PBS buffer.

Pore filter size	50 nm	100 nm	200 nm	MLVs
Heating cycle				
T_m (peak 1) °C	40.5	40.5 ± 0.1	40.4	41.1
T_m (peak 2) °C	41.1	40.9	40.9	
ΔH_m (total) kcal/mol	5.8	6.5 ± 0.3	6.9	8.9
ΔS_m (total) kcal/(mol K)	0.018	0.021	0.022	0.028
ΔS_m (total) J/(mol K)	77.4	86.8	92.4	119.0
Cooling cycle				
T_c °C	40.9	40.9	40.9	41.5
ΔH_c (total) kcal/mol	5.9	6.6	7.0	8.7
ΔS_c (total) kcal/(mol K)	0.019	0.021	0.022	0.028
ΔS_c (total) J/(mol K)	79.2	88.0	92.8	116.1

3.2. Cryo-TEM images

Insight into the origin of the multiple peaks comes from cryo-TEM images of the samples. Extrusion of the DMPC MLVs through the 400 nm polycarbonate filter 10× results in a large range of vesicle types: large and small multivesicular vesicles (MVVs), oligolamellar vesicles, and both large (>200 nm) and small unilamellar vesicles (Fig. 6). Further extrusion changes the vesicle population to one similar to that for vesicles extruded through the 200 nm polycarbonate filter (40×), where smaller structures with the same types (MVVs, oligolamellar and unilamellar) of vesicles are observed (Fig. 7A). Previous work has also shown the development of vesicles within vesicles and the persistence of lamellarity during preparation of smaller vesicles from MLVs by extrusion through 200 nm pore size filters under pressure [13]. In the case of DOPC LUVs, where only an extrusion technique was used (with 1, 0.4 and 0.2 μm filters) [41], cryogenic-transmission electron microscopy (cryo-TEM) showed vesicles within vesicles [24]. The closure of flat interdigitated bilayers above T_m also entrapped smaller vesicles forming MVVs [42].

Further extrusion through the 200 nm filter (120×) (Fig. 7B) or sequentially through a 100 nm filter (40×) (Fig. 7C) reduces the numbers of these non-unilamellar structures, and they disappear almost completely after final extrusion through the 50 nm polycarbonate filters (40×) (Fig. 7D). In previous investigations, successive extrusion (after a freeze/thaw process, 3×) through double stacked 5.0, 1.0, 0.4, 0.2, 0.1 and 0.05 μm filters (each only 5×), showed many oligolamellar vesicles even after the last extrusion with the 50 nm pore size filter [22]. Thus, both the filter size and number of passes affect the final distribution of unilamellar and oligolamellar vesicles.

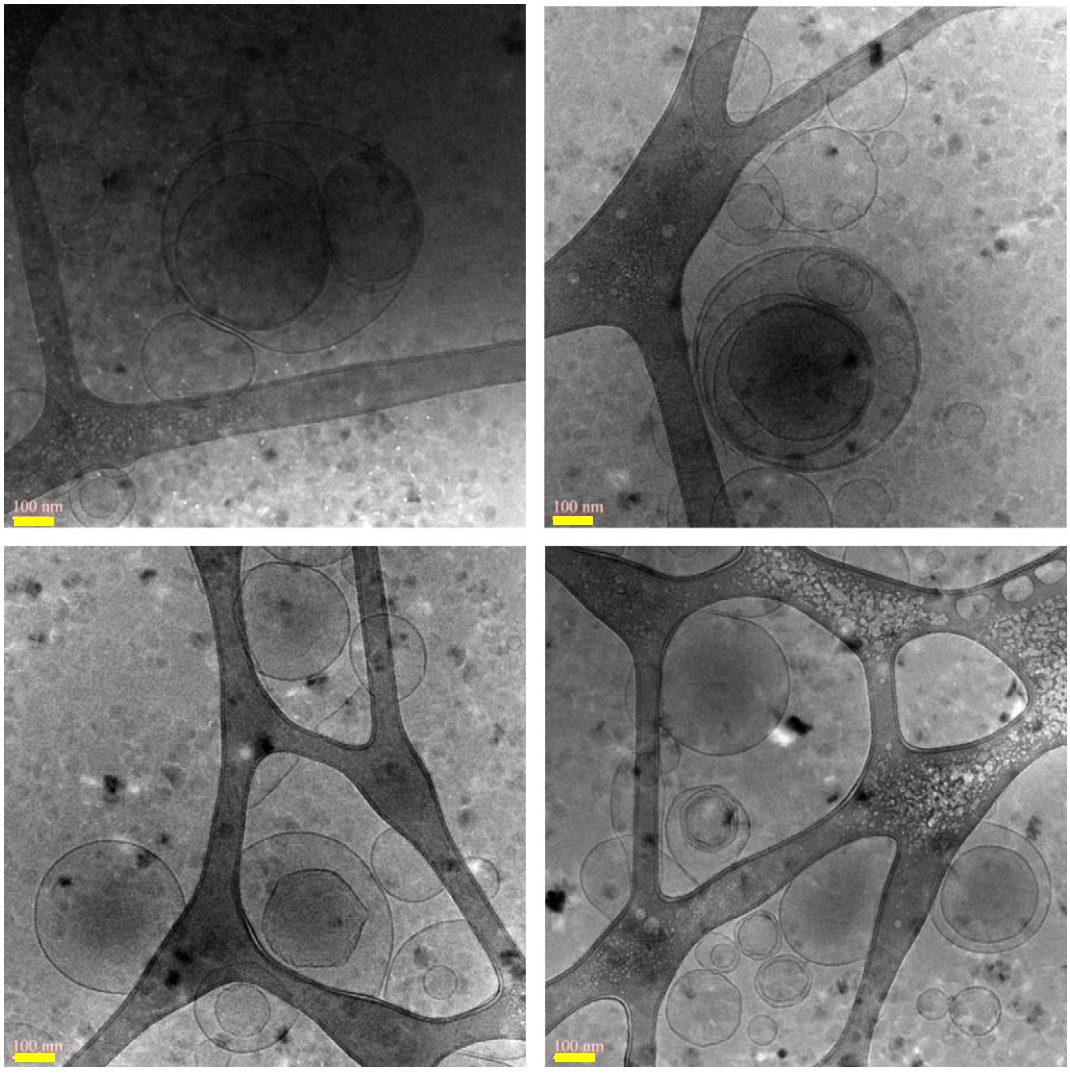

Fig. 6. Cryo-TEM images of DMPC vesicles in water extruded 10× through a 400 nm polycarbonate filter. Structures are large and small unilamellar, oligolamellar and multivesicular vesicles. Scale bars are 100 nm.

The cryo-TEM images also show that the size of the vesicles does not coincide with the pore size of the filters, but does progressively decrease with decreasing pore size, as best seen in the lower magnification images (Fig. 8, all 500 nm scale bar). This can arise since it is known that the nominal pore size is an upper bound for the cylindrical pores in polycarbonate filters used for extrusion (formed by chemical etching along ion tracks [43]) and the average pore size is smaller than the nominal size. It has been shown that the mean vesicle size approaches this pore size as the number of passes and applied pressure increases [16].

Histograms of vesicle sizes taken from ~100 cryo-TEM images/extrusion process for DMPC SUVs/LUVs (Fig. 9) show both the decreased average vesicle size as well as the narrowing of the size distribution after filtrations through successively smaller pore size filters. The sizes decreased from <95.1 nm> to <75.0 nm> to <54.9 nm> as the vesicles were extruded through the 200 nm filter 40×, followed by the 100 nm filter 40× and the 50 nm filter 40× (Table 3). However, increased numbers of passes through the large, 200 nm pore size filter (Fig. 10) have much less effect, decreasing from <95.1 nm> to <90.4 nm> as the number of passes increased from 40 to 120×, with a decrease in the population of the larger size vesicles.

3.3. DLS data

DLS data for DMPC vesicles in water at 25 °C extruded sequentially through 200, 100 and 50 nm (each 40×) polycarbonate filters are shown in Fig. 11, plotted by intensity, volume and number averages. DLS for a tip sonicated sample (15 min) is presented after 1 h. Time dependent data are given in SI Fig. 4.

The z- (D_z), intensity, volume and number averages (Table 3) all show that the vesicle size decreases with a decreasing pore size filter used for the extrusion. The intensity average is weighted to larger vesicles, and the widths become narrower (as indicated by the polydispersity indices, PDI) as the vesicles are extruded through smaller pore size filters. The cumulant analysis by volume percent shows a bimodal distribution for vesicles extruded through the 200 nm pore size filter, and there is a tail for large size vesicles when extruded subsequently through the 100 nm pore size filter. When analyzed by number, there

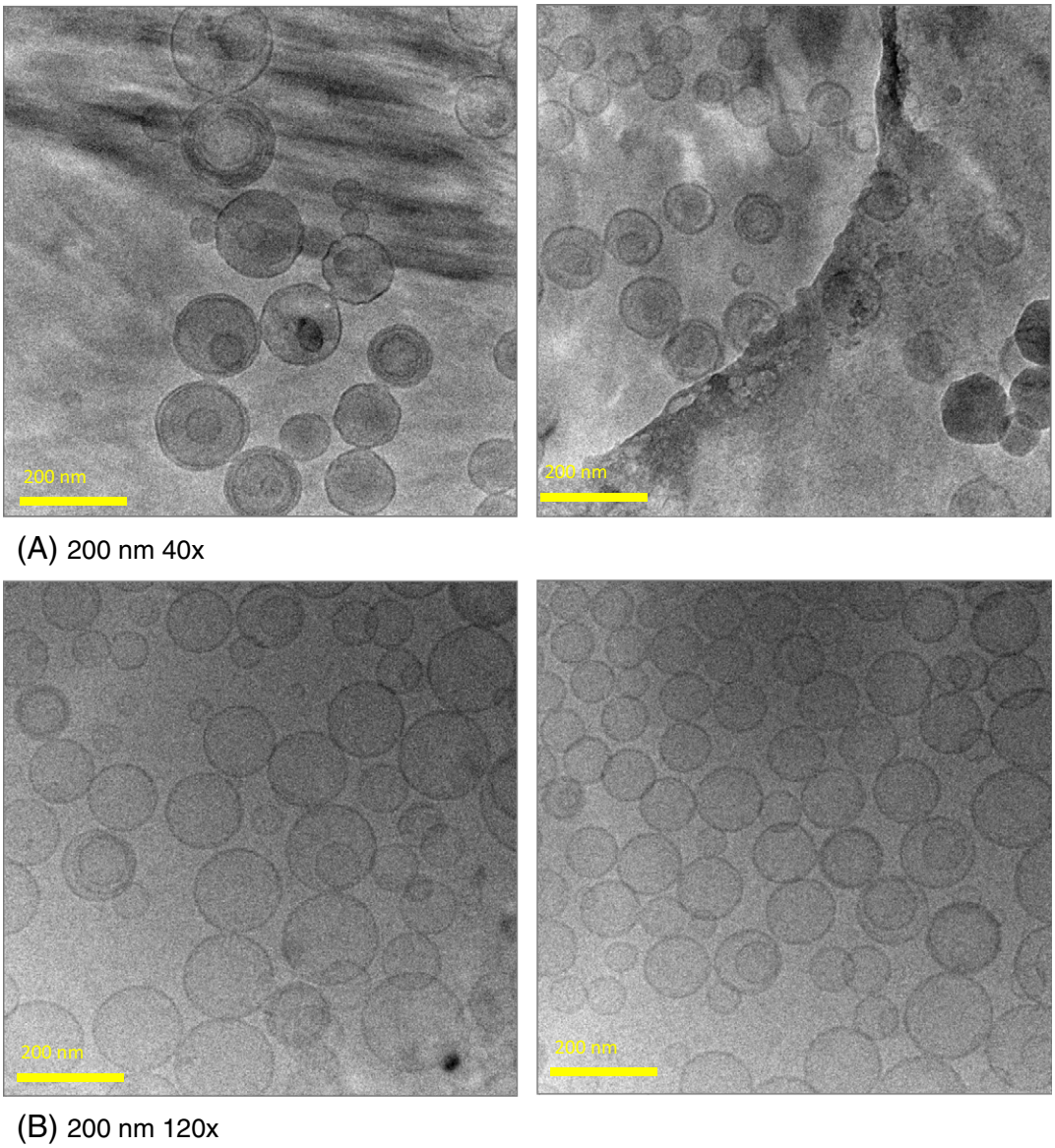

Fig. 7. Cryo-TEM images of DMPC vesicles in water: (A) extruded through a 200 nm pore size filter 40×; (B) extruded through a 200 nm pore size filter 120×; (C) extruded sequentially, 40× each, through 200 nm and 100 nm pore size filters; and (D) extruded sequentially, 40×, each through 200 nm, 100 nm and 50 nm filters. Scale bars are 200 nm.

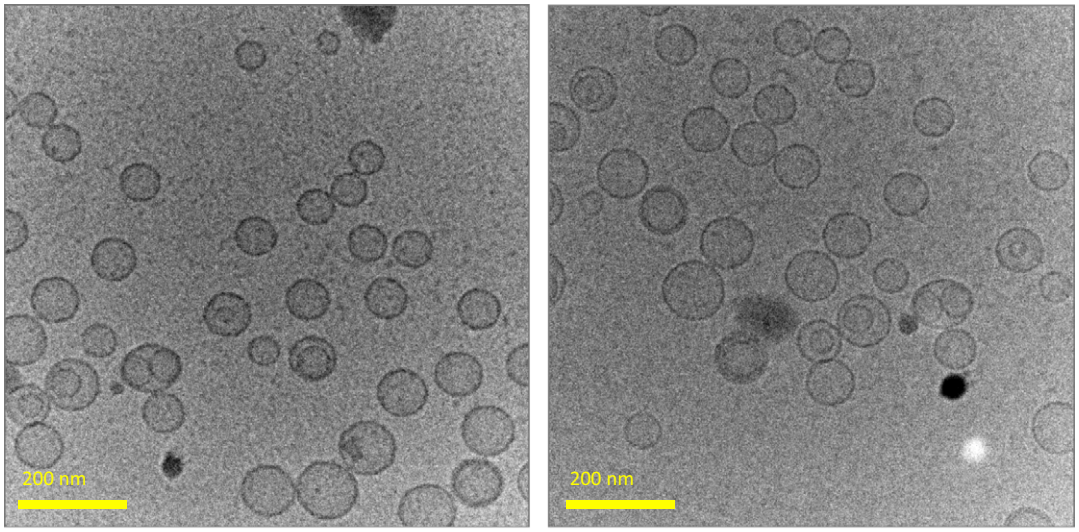

(C) 200 nm 40x and 100 nm 40x

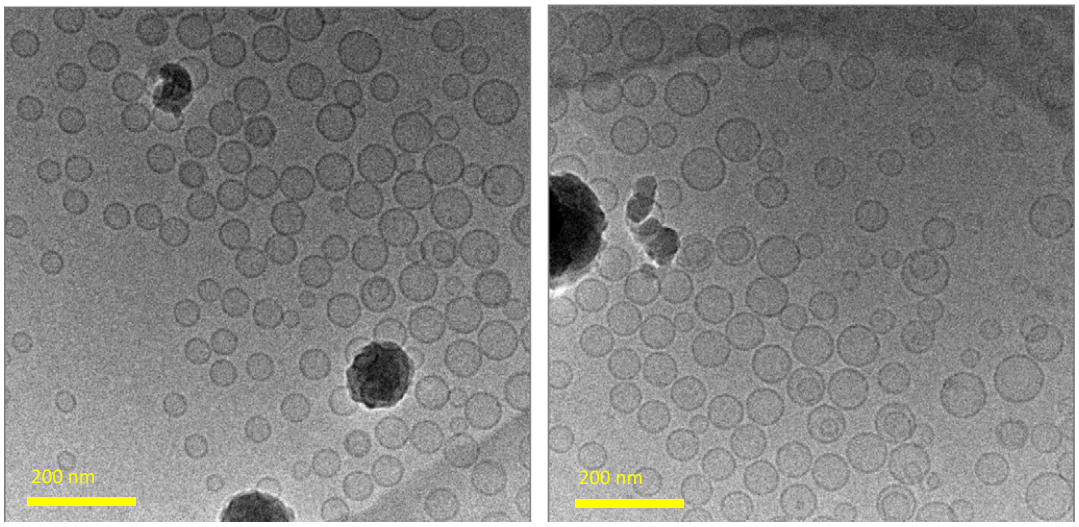

(D) 200 nm 40x, 100 nm 40x and 50 nm 40x

Fig. 7 (*continued*).

are many fewer large vesicles in all cases, although a long tail (at large sizes) is observed for the vesicles extruded with the 200 nm filter. There is good agreement between the number average size measured by DLS and the average obtained from the TEM images. Since the conversion to volume and number averages is based on assumptions (e.g. all particles are spherical and homogeneous, and there is no error in the intensity distribution), the volume and number distributions derived from intensity distributions are useful for estimating relative proportions of species in a multimodal distribution, and are useful for comparative purposes, but are not considered absolute [44]. While the volume distribution is best for characterizing vesicles, comparison with TEM requires the number distribution. From Table 3, the agreement is best for the number distributions. However, conversion of intensity/volume distributions to number distributions can have large errors at the low end of the size distribution because small amounts of particles on a volume basis produce large numbers of particles in the number distribution (due to the $1/10^3$ volume/number ratio).

In the case of the extruded vesicles, as was observed from the cryo-TEM images, the size of the vesicles does not correspond to the nominal diameters of the polycarbonate filters. In general, differences in particle sizes obtained by TEM and DLS arise since DLS measures the hydrodynamic diameter, which includes the solvent moving with the SUVs/LUVs, while TEM does not. The largest discrepancy between pore size and vesicle size, found for the 200 nm pore size filters, has been previously observed [16].

DLS data for DMPC vesicles in water at 25 °C extruded through the 200 nm polycarbonate filter between 5× and 120× are presented in Fig. 12 and Table 2 for the intensity, volume and number averages. Unlike vesicles extruded successively through several filter sizes, the intensity averages as a function of the number of passes through the same 200 nm filter are all very similar; only the vesicles extruded 5× clearly show intensity for very small (~30 nm) vesicle sizes. The vesicles extruded 5× exhibit three maxima in the volume distribution, at ~30, 100 and 200 nm, with the number distribution showing a preponderance of small vesicles. This is consistent with a mechanism in which the large vesicles, after extrusion through the 200 nm (or 400 nm) filter contain many residual smaller vesicles that have been removed from the larger vesicles during the extrusion process. These small vesicles can be seen in Fig. 6 (as shown for the 400 nm filter) along with the larger structures.

After further extrusion through the 200 nm pore size filter (Fig. 12) the number of unstable (<30 nm) SUVs decreases, possibly as the result

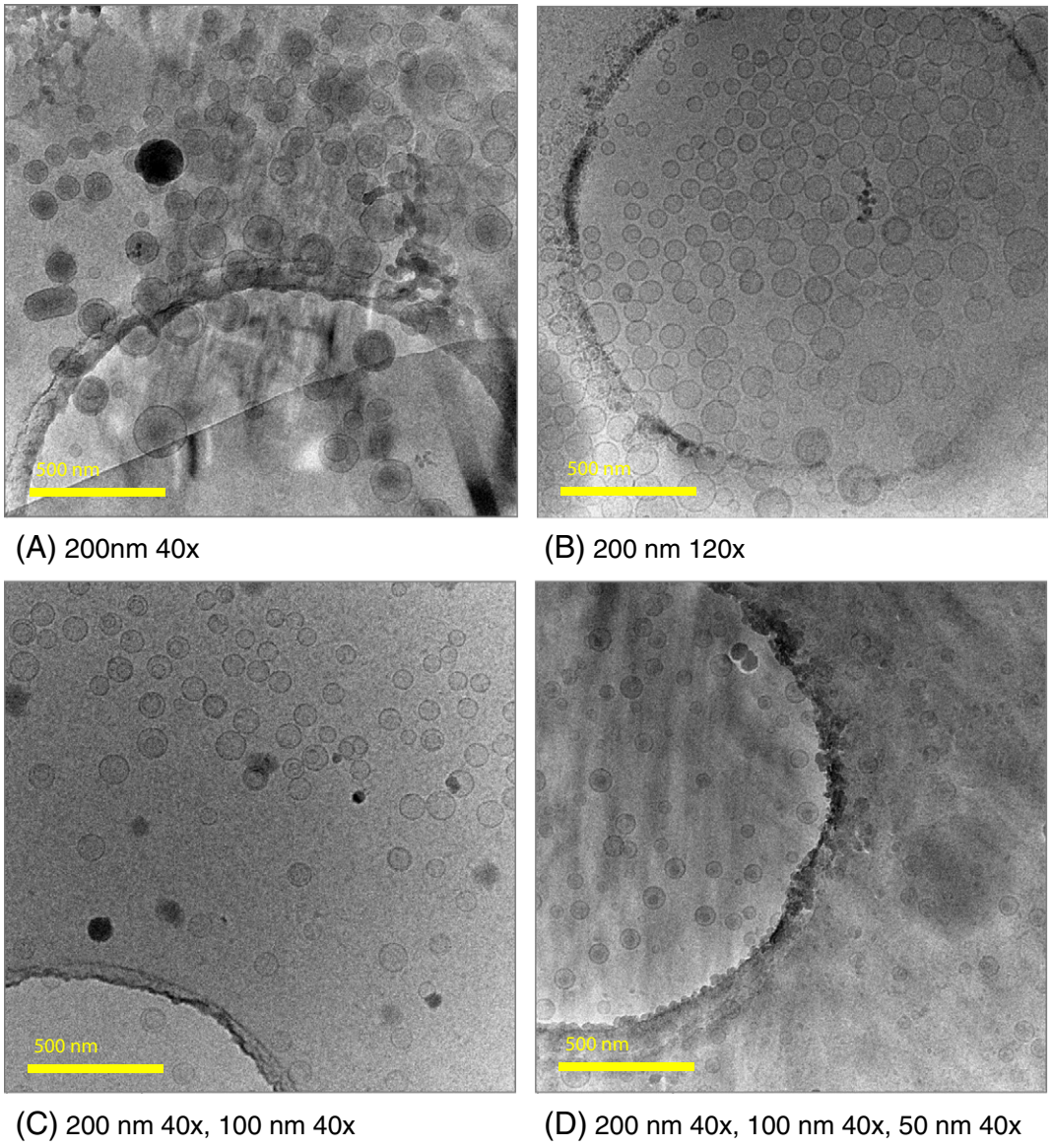

Fig. 8. Cryo-TEM images of DMPC vesicles in water extruded through the: (A) 200 nm pore size filter 40× and (B) 120×; (C) sequentially through the 200 nm and 100 nm filters 40× each; and (D) sequentially through the 200 nm, 100 nm, and 50 nm pore size filters 40× each. Scale bars are 500 nm.

of fusion to form larger (e.g. 60–70 nm) stable vesicles. As the number of passes through the 200 nm filter increases, the ~200 nm vesicles are successively reduced in number (as measured by the peak height intensity in the volume distribution), while the peak at ~100 nm increases in intensity and at the same time moves to smaller vesicle sizes. The increase in the number of smaller vesicles with the number of passes through the filter can clearly be seen in the cumulant analysis by number. The decrease in size, of both the ~200 nm and ~100 nm vesicles is confirmed by cryo-TEM images of vesicles extruded 40× (Fig. 7A) and 120× (Fig. 7B) through the 200 nm filter.

The DLS data for tip sonicated DMPC SUVs (Fig. 12, SI Fig. 4 and SI Table 1) show the decrease of large size vesicles (at >1000 nm and ~200 nm) and the increase in the vesicles at ~30 nm with sonication time. Although we did not obtain cryo-TEM images for these samples, the observed nano-DSC doublet is also assigned to unilamellar and oligolamellar vesicles. In previous work on single component vesicles prepared by sonication to clarity, two or three vesicle populations have been observed. Sonicated DPPC [10] and DSPC [45] SUVS indicate that there is extensive and rapid fusion [25,33,46,45] to products in a wide range of sizes, characteristic of the original small SUVs (~30 nm), ~100 nm LUVs and a large population characteristic of very large structures, attributed to MLV contamination [32].

4. Discussion

The purpose of this investigation was to elucidate the reason(s) for the double phase transition temperatures observed in small single component vesicles obtained from parent multilamellar vesicles. Since vesicles >70 nm are stable below T_m [46], DLS, nano-DSC and TEM images can be better correlated for extruded vesicle populations. The current results show two transitions for extruded or freeze/thawed and extruded vesicles in which the higher temperature peak for DMPC increases with respect to the lower temperature peak (near that of the parent MLVs) as the LUVs decrease in size and as fewer oligolamellar structures are observed by cryo-TEM imaging. DLS and TEM data confirmed that the LUVs contained no residual large, micron size MLVs. Further, the high temperature transition increased in temperature with decreased LUV size, and after extrusion with the 50 nm pore size filter was a single peak. When the LUVs were extruded with the same pore size filter for

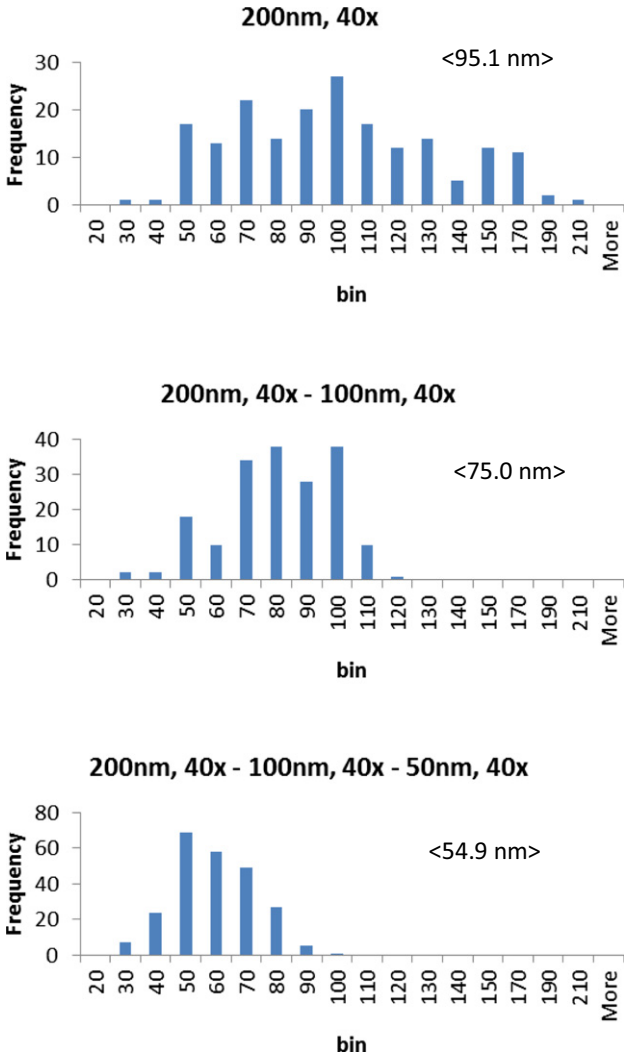

Fig. 9. Histograms of vesicle sizes measured from cryo-TEM images of MLVs extruded successively through 200 nm, 100 nm and 50 nm pore size filters. Average sizes in brackets.

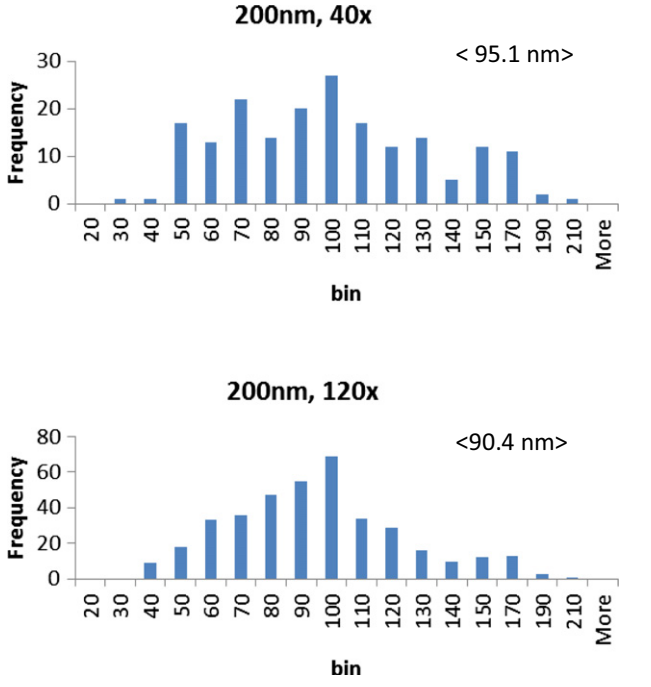

Fig. 10. Histograms of vesicle sizes measured from cryo-TEM images of MLVs extruded successively through a 200 nm filter 40× and 120×. Average sizes in brackets.

different numbers of passes, the positions of the two peaks were constant, but differed in relative intensity.

Thus, the main difference between vesicles prepared using different extrusion filters and number of extrusions is the relative number of unilamellar, oligolamellar and multivesicle (MVVs) vesicles. The combined nano-DSC and cryo-TEM results strongly suggest that the origin of the double transitions arises from vesicles which have or do not have oligolamellar morphologies. Although extrusion should produce unilamellar vesicles, the results presented here, as well as in many other reports in the literature show that oligolamellar and multivesicle vesicles [47,48] often form. We expect that MVVs will have transition temperatures characteristic of the individual bilayers, since the exterior and enclosed vesicles are not in contact with each other. Therefore, we assign the lower temperature transition observed for the DMPC SUVs/LUVs to vesicles in which there are still some double or multiple bilayers; this peak decreases in relative intensity compared with the high temperature peak (e.g. for the nominal 200 nm vesicles extruded 40× versus 120×) as the number of these structures decreases, and as the sonication time increases. The higher temperature peak in DMPC SUVs/LUVs is then assigned to SUVs/LUVs with only a single bilayer in contact with a bulk aqueous phase on both sides. This peak increases in temperature as the vesicle size decreases. For DPPC extruded vesicles, the higher temperature peak occurs at a temperature of the parent MLV peak and the lower temperature peak decreases as the filters used for extrusion decrease in size.

We note that for the LUVs, T_m is higher for DMPC and lower for DPPC than the parent MLVs. These differences have been observed in previous, earlier investigations of unilamellar vesicles, where mainly decreases [1,26,29,49,50] but also increases (DMPC [51], DPPC [33]) in T_m have been associated with smaller vesicles compared with the parent MLVs. Calorimetric data for double calorimetric transitions in extruded PC vesicles [52] show a sharp peak slightly below and a broader peak slightly above 24 °C for extruded DMPC, and a broadened peak below the MLV peak for extruded DPPC vesicles [28].

Table 3
Sizes of vesicles obtained by extrusion and sonication.

	Extrusion times	D_z (nm)	PD	Intensity (nm)	Volume (nm)	Number (nm)	Cryo-TEM (nm)
200 nm	5×	156.5	0.150	185.3	133.8	36.7	
	10×	151.7	0.107	170.3	157.9	111.7	
	20×	147.7	0.088	163.6	152.1	112.3	
	40×	138.0	0.112	156.9	140.1	98.6	95.1
	120×	131.8	0.129	153.2	126.5	79.4	90.4
100 nm	40×*	109.1	0.089	120.1	101.4	79.0	75.0
50 nm	40×**	65.6	0.055	70.4	58.9	50.3	54.9
Tip sonicated		101.2	0.405	167.9	57.5	27.0	

* 40× 200 nm + 40× 100 nm.
** 40× 200 nm + 40× 100 nm + 40× 50 nm.

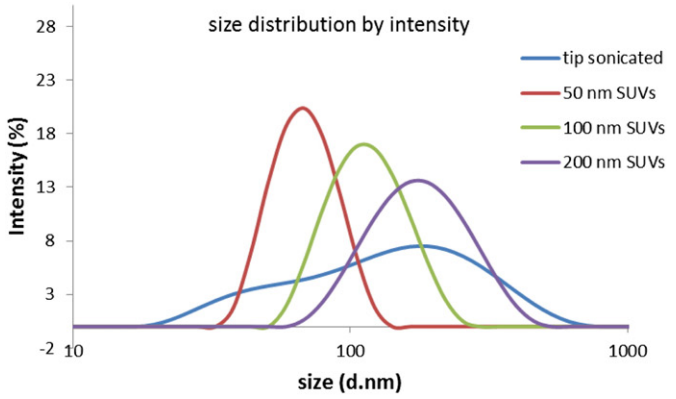

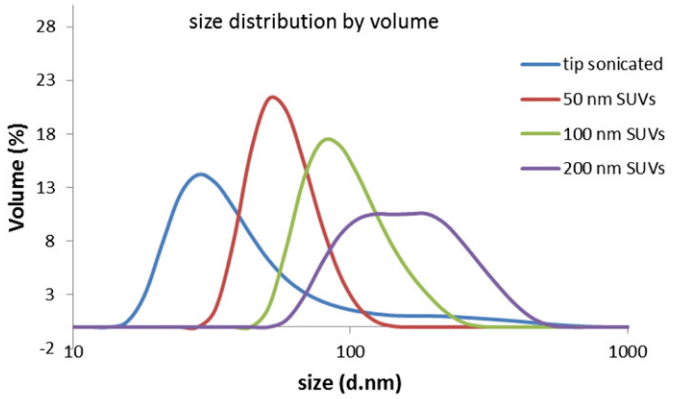

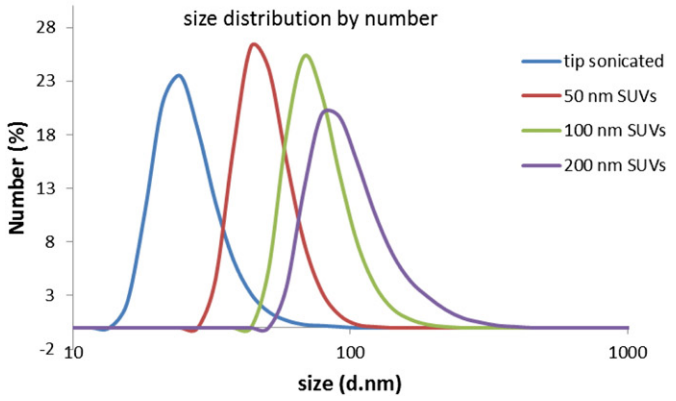

Fig. 11. Dynamic light scattering (DLS) data at 25 °C for 1,2-dimyristoyl-*sn*-glycero-3-phosphocholine (DMPC) vesicles in water extruded sequentially through 200, 100 and 50 nm polycarbonate filters, and sonicated vesicles 1 h after sonication stopped, shown by intensity, volume and number averages.

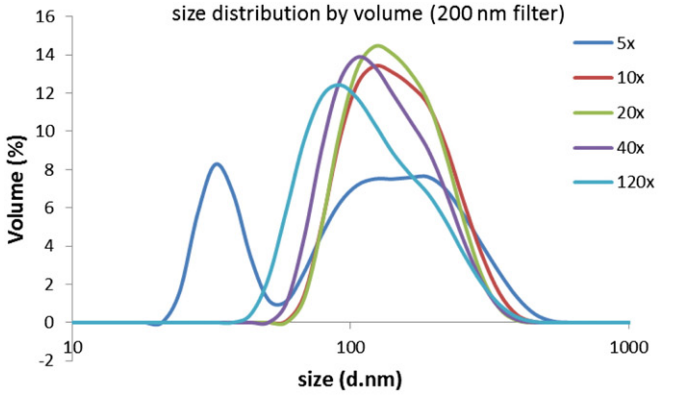

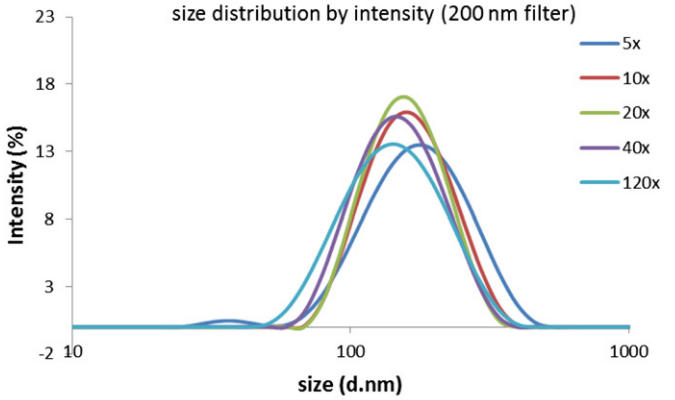

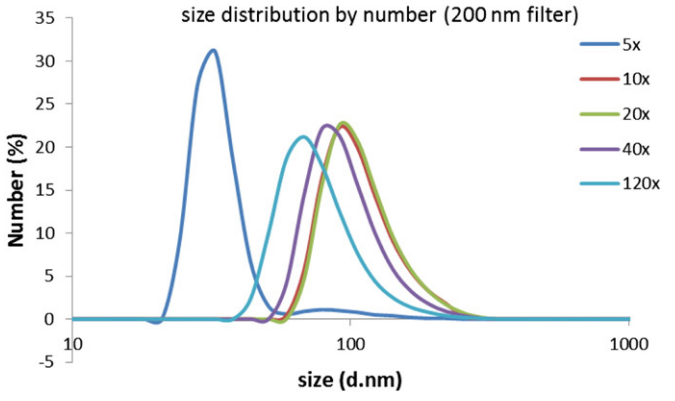

Fig. 12. Dynamic light scattering (DLS) data at 25 °C for 1,2-dimyristoyl-*sn*-glycero-3-phosphocholine (DMPC) vesicles in water extruded sequentially through a 200 nm polycarbonate filter between 5 and 120×, presented by intensity, volume and number averages.

In order to understand the differences between DMPC and DPPC, it is necessary to consider the enthalpies and entropies of the transitions. Since $T_m = \Delta H/\Delta S$, the relative increase or decrease of T_m for unilamellar vesicles compared with oligolamellar or multilamellar vesicles simply reflects subtle differences in the relative contributions of ΔH and ΔS, which are chain length dependent. In fact, both ΔH and ΔS are greater for the longer chain length DPPC (Table 2) than the shorter chain length DMPC (Table 1). However, T_m is the ratio of ΔH to ΔS, which will depend on the relative contributions of the two terms, so that their ratio may fall above or below the parent MLVs.

In the current investigation it was not possible to quantify the populations of vesicles associated with the two phase transition temperatures, since the relative number of single/multiple bilayers is not known, and therefore the contribution to the enthalpy/entropy of the individual components cannot be determined. However, for ΔH (total) and ΔS (total), both ΔH (LUVs) < ΔH (MLVs), and ΔS (LUVs) < ΔS (MLVs), and both decrease as a function of decreased vesicle size for both DMPC and DPPC. Previously, it has been shown that ΔS is less for MLVs than for alkane chain melting, indicating that instead of a change from a true crystal to a disordered melt (alkanes), the gel and fluid phases are more similar to each other and there is more disorder in the gel phase of lipids in MLVs than in alkanes [50]. Here, since $\Delta S = S_{liqxtal} - S_{gel}$, this now implies that the packing of the lipids in the gel phase of the SUVs is more similar to that of the fluid phase than is the case for the MLVs, i.e. the SUVs/LUVs become more disordered and similar to the fluid phase as the vesicle size decreases. The decrease in order with vesicle size also results in lower values of ΔH(total) with vesicle size, and all are less than the more ordered MLVs. Lower transition enthalpies and entropies have been measured for SUVs/LUVs compared with the parent MLVs [25,50,53,54], and have been attributed to curvature induced [29,55] decreased lateral packing [56] and interchain

interactions [57] observed by Raman spectroscopy and increased alkyl chain disorder (trans/gauche isomerism) observed by Raman [57,58] and NMR [7,59,60] spectroscopy.

The widths (full widths at half height) of the DMPC and DPPC MLV phase transitions are narrower than those of the SUVs/LUVs, but except for the vesicles extruded with 50 nm pore size filters, this is partially due to the overlap of single and oligovesicular species. In the case of LUVs extruded finally with the 50 nm pore size filter, the FWHM is broader than for the MLVs. The narrower half widths for the MLVs compared with the unilamellar vesicles have been suggested to result from the lower curvature of the MLVs [30,61] and/or from increased cooperativity of the transition due to interbilayer interactions [28].

It has previously been suggested that each transition envelop for the MLVs and SUVs/LUVs was not a superposition of the transition curves of a distribution of vesicle sizes, each with its own T_m [29]. The widths of both MLVs and SUVs/LUVs were instead attributed to a mixed population of gel and liquid crystalline clusters/aggregates within a single bilayer during the transition [29], with the narrower MLV transition having a limiting finite width of ~0.076 K [29]. For MLVs/(LUVs or SUVs), there are a smaller/larger number of larger/smaller size clusters, with a smaller/larger fraction of "mismatched" lipids, i.e. those in which a more ordered gel phase lipid is next to a less ordered fluid phase lipid with different interaction energies [29,55]. The smaller size of the "cooperative unit" in the LUVs/SUVs, attributed to a reduction in the effective range of interactions between lipid molecules within a single bilayer, was suggested to be due to less ordered molecular packing, which in turn was due to their smaller radii of curvature. In addition to this possible explanation (which we cannot verify), it may be necessary to consider not only interactions within single bilayers, but also inter-bilayer interactions. Bilayers in MLVs are (except for the outer- and inner-most bilayers) bounded by two adjacent bilayers, while LUVs or SUVs are bounded by bulk water on either side of the single bilayer. The bilayer separation in MLVs, typically ~2.5 nm (~35 water molecules/phospholipid) is the result of a balance between repulsive electrostatic, hydration and steric forces and attractive van der Waal attractions. These differences in interbilayer interactions may contribute to the differences in phase behavior between the MLVs and unilamellar vesicles, and account for the difference in widths of the MLV and LUV/SUV transitions.

The results for the DMPC and DPPC unilamellar vesicles are not consistent with an interpretation where the two transitions result from decoupled, separate transitions from the inner and outer leaflets of the bilayer. The inequality between the number of lipids in the inner and outer leaflets will increase as the vesicle size decreases, with the outer, less curved leaflet having a transition temperature closer to that of the MLVs. Therefore, the intensity of the transition near that of the MLV transition should increase with decreasing vesicle size, a trend not observed either for the DMPC or DPPC unilamellar vesicles. Further, lipids extruded with the 50 nm pore size filter, where cryo-TEM images show only unilamellar vesicles, have only a single T_m. (This peak is asymmetric, and an attempt to model this asymmetry is underway.) Thus, the current results indicate that it is not possible to distinguish between the inner and outer leaflets of SUVs/LUVs based on calorimetric methods, although previous NMR and fluorescence measurements have shown that the inner and outer leaflets of these unilamellar vesicles have different signatures. Differences between the two leaflets of the bilayer for single component vesicles have been observed by ^{31}P NMR using shift reagents [33,62], fluorine NMR with and without addition of paramagnetic ions [63] and ^{1}H-NMR for sonicated egg lecithin with [64,65] and without a shift reagent [66].

The coupling between the two leaflets of the bilayer in MLVs, LUVs and SUVs is unlike the case of supported lipid bilayers (SLBs), where there is at least one report of separate calorimetric phase transitions for the proximal (near support) and distal (near aqueous phase) leaflets [31].There is also considerable atomic force microscopy (AFM) evidence for different transition temperatures for the proximal and distal leaflet bilayers in planar SLBs [67–69].

Lastly, the data suggest that repeated use of a single pore size filter cannot produce unilamellar vesicles (except when extruded with pore filters <50 nm) of a size corresponding to the pore size employed. This is particularly true for the larger filters, e.g. 200 nm, where a very large number of transits (120×) through the extruder has only a small effect on the size/size distribution, although it does reduce the number of oligolamellar vesicles. Only the 50 nm pore size filter produced unilamellar vesicles, with nearly unilamellar vesicles produced for the 100 nm pore size filter.

5. Conclusions

DMPC and DPPC vesicles were prepared from multilamellar vesicles by an extrusion method (with and without a freeze/thaw cycle) using polycarbonate filters with pore sizes ranging from 50 to 400 nm, or by sonication, and characterized nano-differential scanning calorimetry, dynamic light scattering and cryo-TEM. When two gel-to-liquid crystal phase transition temperatures are observed, they were not the result of decoupled phase transitions between the inner and outer leaflets of the vesicles. Instead, they have been attributed to mixtures of single bilayer and oligolamellar vesicles, where the transition temperatures may be affected both by curvature effects and whether the bilayers are bounded by free water (or buffer) or by adjacent bilayers. The oligolamellar vesicles were assigned T_ms close to those of the MLVs, and the other T_m was assigned to the unilamellar vesicles. However, the relative positions of the transition temperatures of the unilamellar vesicles with respect to those of the parent MLVs depend on subtle differences in the enthalpies, ΔH, and entropies, ΔS, of melting (since $T_m = \Delta H/\Delta S$). Both the enthalpies and entropies of melting decreased with decreasing vesicle size for DMPC and DPPC. In the case of DPPC, T_m for the unilamellar vesicles decreased with decreased vesicle size, while for DMPC, T_m for the unilamellar vesicles increased with decreased vesicle size. For DMPC vesicles finally extruded with the 50 nm polycarbonate filter, only a single T_m was observed, and cryo-TEM images showed only unilamellar and no oligolamellar vesicles. For vesicles extruded with the 400 nm, 200 nm and 100 nm pore size filters, it was not possible to eliminate these oligolamellar structures even after many passes (40× to 120×), although the effect was not large for the vesicles extruded using the 100 nm pore size filter. These effects should be considered when assigning calorimetric phase transition temperatures. DLS data cannot be used to indicate the presence of oligolamellar vesicles.

Appendix A. Supplementary data

Supplementary data to this article can be found online at http://dx.doi.org/10.1016/j.bbamem.2014.10.003.

References

[1] R.L. Biltonen, D. Lichtenberg, The use of differential scanning calorimetry as a tool to characterize liposome preparations, Chem. Phys. Lipids 64 (1993) 129–142.
[2] J.W.V. Lasch, M. Brandl, Preparation of liposomes, in: V. Torchilin, V. Weissig (Eds.), Liposomes: A Practical Approach, Oxford University Press, Oxford/New York, 2003, pp. 3–30.
[3] A.D. Bangham, M.M. Standish, J.C. Watkins, Diffusion of univalent ions across lamellae of swollen phospholipids, J. Mol. Biol. 13 (1965) 238–252.
[4] P.L. Luisi, P. Walde, Giant Vesicles, 1990. (New York City: Wiley).
[5] J.H. Lee, V. Agarwal, A. Bose, G.F. Payne, S.R. Raghavan, Transition from unilamellar to bilamellar vesicles induced by an amphiphilic biopolymer, Phys. Rev. Lett. 96 (2006).
[6] E.G. Finer, A.G. Flook, H. Hauser, Mechanism of sonication of aqueous egg-yolk lecithin dispersions and nature of resultant particles, Biochim. Biophys. Acta 260 (1972) 49–58.
[7] M.P. Sheetz, S.I. Chan, Effect of sonication on structure of lecithin bilayers, Biochemistry 11 (1972) 4573–4581.
[8] D. Papahadjopoulos, G. Poste, B.E. Schaeffer, W.J. Vail, Membrane fusion and molecular segregation on phospholipid vesicles, Biochim. Biophys. Acta 352 (1974) 10–28.

[9] Y. Barenholz, D. Gibbes, B.J. Litman, J. Goll, T.E. Thompson, F.D. Carlson, Simple method for preparation of homogeneous phospholipid vesicles, Biochemistry 16 (1977) 2806–2810.
[10] C.-H. Huang, Phosphatidylcholine vesicles. Formation and physical characteristics, Biochemistry 8 (1969) 344–352.
[11] F. Olson, C.A. Hunt, F.C. Szoka, W.J. Vail, D. Papahadjopoulos, Preparation of liposomes of defined size distribution by extrusion through polycarbonate membranes, Biochim. Biophys. Acta 557 (1979) 9–23.
[12] M.J. Hope, M.B. Bally, G. Webb, P.R. Cullis, Production of large unilamellar vesicles by a rapid extrusion procedure—characterization of size distribution, trapped volume and ability to maintain a membrane potential, Biochim. Biophys. Acta 812 (1985) 55–65.
[13] B. Mui, L. Chow, M.J. Hope, Extrusion technique to generate liposomes of defined size, Liposomes Part A 367 (2003) 3–14.
[14] M.J. Hope, M.B. Bally, L.D. Mayer, A.S. Janoff, P.R. Cullis, Generation of multilamellar and unilamellar phospholipid vesicles, Chem. Phys. Lipids 40 (1986) 89–107.
[15] L.D. Mayer, M.J. Hope, P.R. Cullis, Vesicles of variable sizes produced by a rapid extrusion procedure, Biochim. Biophys. Acta 858 (1986) 161–168.
[16] P.J. Patty, B.J. Frisken, The pressure-dependence of the size of extruded vesicles, Biophys. J. 85 (2003) 996–1004.
[17] Y.P. Patil, M.D. Kumbhalkar, S. Jadhav, Extrusion of electroformed giant unilamellar vesicles through track-etched membranes, Chem. Phys. Lipids 165 (2012) 475–481.
[18] L.D. Mayer, M.J. Hope, P.R. Cullis, A.S. Janoff, Solute distributions and trapping efficiencies observed in freeze–thawed multilamellar vesicles, Biochim. Biophys. Acta 817 (1985) 193–196.
[19] L.D. Mayer, M.J. Hope, P.R. Cullis, A.S. Janoff, Solute distributions and trapping efficiencies observed in freeze–thawed multilamellar vesicles, Biochim. Biophys. Acta 817 (1985) 193–196.
[20] K.A. Edwards, A.J. Baeumner, Analysis of liposomes, Talanta 68 (2006) 1432–1441.
[21] M. Frohlich, V. Brecht, R. Peschka-Suss, Parameters influencing the determination of liposome lamellarity by P-31-NMR, Chem. Phys. Lipids 109 (2001) 103–112.
[22] N. Berger, A. Sachse, J. Bender, R. Schubert, M. Brandl, Filter extrusion of liposomes using different devices: comparison of liposome size, encapsulation efficiency, and process characteristics, Int. J. Pharm. 223 (2001) 55–68.
[23] P.Y. Bolinger, D. Stamou, H. Vogel, Integrated nanoreactor systems: triggering the release and mixing of compounds inside single vesicles, J. Am. Chem. Soc. 126 (2004) 8594–8595.
[24] O. Le Bihan, P. Bonnafous, L. Marak, T. Bickel, S. Trepout, S. Mornet, et al., Cryo-electron tomography of nanoparticle transmigration into liposome, J. Struct. Biol. 168 (2009) 419–425.
[25] J. Suurkuusk, B.R. Lentz, Y. Barenholz, R.L. Biltonen, T.E. Thompson, Calorimetric and fluorescent probe studies of gel–liquid crystalline phase transition in small, single lamellar dipalmitoylphosphatidylcholine vesicles, Biochemistry 15 (1976) 1393–1401.
[26] B.R. Lentz, Y. Barenholz, T.E. Thompson, Fluorescence depolarization studies of phase transitions and fluidity in phospholipid bilayers. 1. Single component phosphatidylcholine liposomes, Biochemistry 15 (1976) 4521–4528.
[27] D. Lichtenberg, M. Menashe, S. Donaldson, R.L. Biltonen, Thermodynamic characterization of the pretransition of unilamellar dipalmitoyl-phosphatidylcholine vesicles, Lipids 19 (1984) 395–400.
[28] T. Heimburg, Mechanical aspects of membrane thermodynamics. Estimation of the mechanical properties of lipid membranes close to the chain melting transition from calorimetry, Biochim. Biophys. Acta Biomembr. 1415 (1998) 147–162.
[29] R.L. Biltonen, A statistical–thermodynamic view of cooperative structural changes in phospholipid bilayer membranes — their potential role in biological function, J. Chem. Thermodyn. 22 (1990) 1–19.
[30] S. Ahmed, S.L. Wunder, Effect of high surface curvature on the main phase transition of supported phospholipid bilayers on SiO_2 nanoparticles, Langmuir 25 (2009) 3682–3691.
[31] J. Yang, J. Appleyard, The main phase transition of mica-supported phosphatidylcholine membranes, J. Phys. Chem. B 104 (2000) 8097–8100.
[32] H.L. Kantor, S. Mabrey, J.H. Prestegard, J.M. Sturtevant, Calorimetric examination of stable and fusing lipid bilayer vesicles, Biochim. Biophys. Acta 466 (1977) 402–410.
[33] D. Lichtenberg, E. Freire, C.F. Schmidt, Y. Barenholz, P.L. Felgner, T.E. Thompson, Effect of surface curvature on stability, thermodynamic behavior and osmotic activity of dipalmitoylphosphatidylcholine single lamellar vesicles, Biochemistry 20 (1981) 3462–3467.
[34] Avanti Polar Lipids, Determination of total phosphorus, Technical Support, Analytical Procedures, 2014.
[35] C.H. Fiske, Y. Subbarow, The colorimetric determination of phosphorus, J. Biol. Chem. 66 (1925) 375–400.
[36] P.S. Chen, T.Y. Toribara, H. Warner, Microdetermination of phosphorus, Anal. Chem. 28 (1956) 1756–1758.
[37] Cumulants Analysis defined in ISO 13321 and ISO 22412; Calculating Vol. Distribution from Dynamic Light Scattering, Malvern Instruments: Worcestershire U, 2007.
[38] R. Lewis, N. Mak, R.N. McElhaney, A differential scanning calorimetric study of the thermotropic phase behavior of model membranes composed of phosphatidylcholines containing linear saturated fatty acyl chains, Biochemistry 26 (1987) 6118–6126.
[39] B. Gruenewald, S. Stankowski, A. Blume, Curvature influence on the cooperativity and the phase transition enthalpy of lecithin vesicles, 1021979. 227–229.
[40] R.O. Brito, E.F. Marques, Neat DODAB vesicles: effect of sonication time on the phase transition thermodynamic parameters and its relation with incomplete chain freezing, Chem. Phys. Lipids 137 (2005) 18–28.
[41] O. Lambert, D. Levy, J.L. Ranck, G. Leblanc, J.L. Rigaud, A new "gel-like" phase in dodecyl maltoside-lipid mixtures: implications in solubilization and reconstitution studies, Biophys. J. 74 (1998) 918–930.
[42] E.T. Kisak, B. Coldren, C.A. Evans, C. Boyer, J.A. Zasadzinski, The vesosome — a multicompartment drug delivery vehicle, Curr. Med. Chem. 11 (2004) 199–219.
[43] R.L. Fleischer, R.B. Price, R.M. Walker, Nuclear Tracks in Solids, University of California Press, Berkeley, CA, 1975.
[44] R. Pecora, Dynamic Light Scattering: Applications of Photon Correlation Spectroscopy, Plenum Press, New York and London, 1985.
[45] A.L. Larrabee, Time-dependent changes in the size distribution of distearoylphasphatidylcholine vesicles, Biochemistry 18 (1979) 3321–3326.
[46] S.E. Schullery, C.F. Schmidt, P. Felgner, T.W. Tillack, T.E. Thompson, Fusion of diplamitoylphosphatidylcholine vesicles, Biochemistry 19 (1980) 3919–3923.
[47] M. Brandl, M. Drechsler, D. Bachmann, C. Tardi, M. Schmidtgen, K.H. Bauer, Preparation and characterization of semi-solid phospholipid dispersions and dilutions thereof, Int. J. Pharm. 170 (1998) 187–199.
[48] G. Rodríguez, G. Soria, E. Coll, L. Rubio, L. Barbosa-Barros, C. López-Iglesias, et al., Bicosomes: bicelles in dilute systems, Biophys. J. 99 (2010) 480–488.
[49] R.C. Spiker, I.W. Levin, Phase transitions of phospholipid single-wall vesicles and multilayers-measurement by vibrational Raman spectroscopic frequency differences, Biochim. Biophys. Acta 433 (1976) 457–468.
[50] D.L. Melchior, J.M. Steim, Thermotropic transitions in biomembranes, Annu. Rev. Biophys. Bioeng. 5 (1976) 205–238.
[51] A. Jutila, P.K.J. Kinnunen, Novel features of the main transition of dimyristoylphosphocholine bilayers revealed by fluorescence spectroscopy, J. Phys. Chem. B 101 (1997) 7635–7640.
[52] A.J. Jin, C.P. Mudd, N.L. Gershfeld, Unusual structural transformations in large unilamellar vesicle suspensions of DMPC by Cp lambda-1 calorimetry, Biophys. J. 74 (1998) A312-A.
[53] J.M. Sturtevant, Some applications of calorimetry in biochemistry and biology, Annu. Rev. Biophys. Bioeng. 3 (1974) 35–51.
[54] P.W.M. Vandijck, B. Dekruijff, P. Aarts, A.J. Verkleij, J. Degier, Phase transitions in phospholipid model membranes of different curvature, Biochim. Biophys. Acta 506 (1978) 183–191.
[55] E. Freire, R. Biltonen, Estimation of molecular averages and equilibrium fluctuations in lipid bilayer systems from excess heat capacity function, Biochim. Biophys. Acta 514 (1978) 54–68.
[56] B.P. Gaber, W.L. Peticolas, On the quantitative interpretation of biomembrane structure by Raman spectroscopy, 4651977. 260–274.
[57] R. Mendelsohn, S. Sunder, H.J. Bernstein, The effect of sonication on the hydrocarbon chain conformation in model membrane systems: a Raman spectroscopic study, Biochim. Biophys. Acta Biomembr. 419 (1976) 563–569.
[58] R.C. Spiker, I.W. Levin, Effect of bilayer curvature on vibrational raman spectroscopic behavior of phospholipid–water assemblies, Biochim. Biophys. Acta 455 (1976) 560–575.
[59] D. Lichtenberg, N.O. Petersen, J.L. Girardet, M. Kainosho, P.A. Kroon, C.H.A. Seiter, et al., Interpretation of proton magnetic resonance linewidths for lecithin dispersions—effect of particle size and chain packing, Biochim. Biophys. Acta 382 (1975) 10–21.
[60] N.O. Petersen, S.I. Chan, More on motional state of lipid bilayer membranes — interpretation of order parameters obtained from nuclear magnetic resonance experiments, Biochemistry 16 (1977) 2657–2667.
[61] T. Brumm, K. Joergensen, O.G. Mouritsen, T.M. Bayerl, The effect of increasing membrane curvature on the phase transition and mixing behavior of a dimyristoyl-*sn*-glycero-3-phosphatidylcholine/distearoyl-*sn*-glycero-3-phosphatidylcholine lipid mixture as studied by Fourier transform infrared spectroscopy and differential scanning calorimetry, Biophys. J. 70 (1996) 1373–1379.
[62] A. Chrzeszczyk, A. Wishnia, C.S. Springer Jr., The intrinsic structural asymmetry of highly curved phospholipid bilayer membranes, 4701977. 161–169.
[63] K.J. Longmuir, F.W. Dahlquist, Direct spectroscopic observation of inner and outer hydrocarbon chains of lipid bilayer vesicles, Proc. Natl. Acad. Sci. U. S. A. 73 (1976) 2716–2719.
[64] R.J. Kostelnik, S.M. Castella, 250-MHz proton magnetic resonance spectrum of a sonicated lecithin dispersion in water-effect of ferricyanide, manganese (II), europium (III) and gadolinium (III) ions on choline methyl resonance, J. Magn. Reson. 7 (1972) 219–223.
[65] J.A. Berden, R.W. Barker, G.K. Radda, NMR-studies on phospholipid bilayers some factors affecting lipid distribution, Biochim. Biophys. Acta 375 (1975) 186–208.
[66] R.J. Kostelnik, S.M. Castella, 250 MHz proton NMR-study of sonicated egg-yolk lecithin dispersions in D_2O. II. Doublet character of resonance signal of choline methyl groups, J. Magn. Reson. 9 (1973) 291–295.
[67] D. Keller, N.B. Larsen, I.M. Moller, O.G. Mouritsen, Decoupled phase transitions and grain-boundary melting in supported phospholipid bilayers, Phys. Rev. Lett. 94 (2005).
[68] Z.V. Feng, T.A. Spurlin, A.A. Gewirth, Direct visualization of asymmetric behavior in supported lipid bilayers at the gel-fluid phase transition, Biophys. J. 88 (2005) 2154–2164.
[69] A. Charrier, F. Thibaudau, Main phase transitions in supported lipid single-bilayer, Biophys. J. 89 (2005) 1094–1101.